Hindawi
Geofluids
Volume 2023, Article ID 4743053, 9 pages
https://doi.org/10.1155/2023/4743053

Research Article

Water Inrush Mechanism in Fault Fracture Zone Based on a Nonlinear Mechanical Model of Three Flow Fields

Hou Dian-chen,[1] Su Xiao-jian,[1] Wang Wen-qiang,[2] Du Feng,[2,3] and Zhao Yu-yao[4]

[1]*Zhaogu No.2 Mine, Henan Energy Coking Coal Company, Jiaozuo, 454000 Henan, China*
[2]*School of Energy Science and Engineering, Henan Polytechnic University, Jiaozuo, 454000 Henan, China*
[3]*Collaborative Innovation Center of Coal Work Safety and Clean High Efficiency Utilization, Jiaozuo, 454000 Henan, China*
[4]*School of Civil Engineering, Henan Polytechnic University, Jiaozuo, 454000 Henan, China*

Correspondence should be addressed to Du Feng; fdu_cumt@126.com and Zhao Yu-yao; 1185832163@qq.com

Received 12 August 2022; Revised 30 December 2022; Accepted 31 March 2023; Published 17 April 2023

Academic Editor: Liang Xin

Water inrush in the working face caused by seepage instability of fault fracture zone is a major disaster which threatens the safety production in a coal mine. Based on the principle of fluid mechanics, a nonlinear mechanical model with three flow fields is established in this paper. Combining with the actual situation of a fault fracture zone in a coal mine, a multicoupled numerical model is built in COMSOL Multiphysics, in order to study the water pressure and flow velocity in the three flow fields and the flow state of fluids in the aquifer and fault under different ratios of fault permeability and aquifer permeability. The research results show that the permeability in the fault fracture zone is an essential factor affecting the danger of water inrush, and the pressure and flow velocity in the boundary zone of the adjacent flow field varies significantly. Besides, the water inrush in the fault fracture zone is a gradual dynamic process, and the fluid flow from the aquifer through the fault gradually changes from a linear flow state into a nonlinear flow state. Meanwhile, the non-Darcy effect increases and decreases with the growth and decrease of the permeability in the fault fracture zone.

1. Introduction

The fault fracture zone is one of the geological engineering types in karst areas in China. The fault fracture zone is the leading cause of water inrush disasters in a coal mine, which poses a significant threat to the safety production of coal mine [1, 2]. The influence of fault fracture zone on water inrush has three main aspects, namely, shortening the distance between coal seams and water-bearing seams, good hydraulic conductivity and water storage, and reducing the strength of rock seams by the destruction of fault structures [3, 4]. Therefore, when the roadway face crosses the fault zone, the fault is affected by mining disturbance and groundwater seepage migration, and it straightforward induces the water inrush disaster. It is of theoretical significance and practical engineering value to simulate the water inrush process in a fault fracture zone and study the water inrush mechanism for the prediction and safe prevention of water inrush in a coal mine.

Many scholars have conducted extensive research on the problem of water inrush hazards from faults encountered during coal seam excavation. According to the nature of faults, Li et al. [5] classified faults into open and closed spots and studied the mechanism of sudden water in both types of responsibilities. Liu and Hu [6] established a flow-solid coupling mathematical model of coal mining on pressurized water, conducted a numerical simulation to analyze the relationship between each fault element and sudden water, and gave the sudden water criterion. Li et al. [7] reproduced

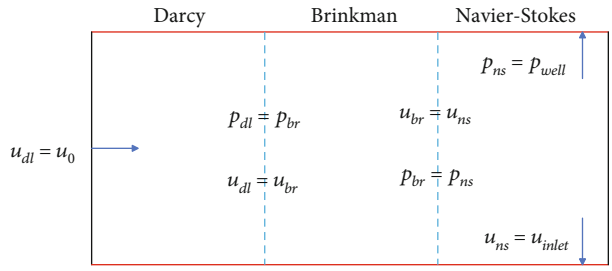

Figure 1: Simplified model of three flow fields.

the process of forming the channel of the coal seam floor containing the fault by numerical simulation based on the physical properties of the blame. They concluded that the respondent's physical properties and the obligation's yield have an important influence on the safety of the coal seam floor. Li et al. [8] established the activation model of the critical layer containing the water barrier, theoretically analyzed the fault activation slip conditions under the action of mineral pressure and water pressure, studied the fault activation syncline mechanism, and obtained the fault activation conditions under the joint effort of mineral stress and water pressure. The above studies mainly focus on the physical properties of faults and fault production. In addition, many scholars have also conducted theoretical analysis and numerical simulation studies on the fault syncline problem from the perspective of fluid mechanics, where fluid enters the fault from the aquifer, which is a nonlinear seepage process. Under the seepage migration effect, the filling particles in the spot are continuously lost, causing the fault permeability and porosity to increase constantly. After excavation disturbance, the fluid breaks through the fault and coal seam boundary and gushes into the coal seam (fluid breaks through the working face into the coal seam), and the syncline disaster occurs [9–11].

Based on a solid engineering background, this paper divides the fluid flow into three stages from the fluid mechanics perspective. Namely, the aquifer laminar flow stage, nonlinear seepage stage in the karst fault, and turbulent flow stage in the roadway flat working face and the flow states of the three steps are described in the finite element software COMSOL Multiphysics using Darcy's law, Forchheimer's modified Brinkman equation, and the Navier-Stokes equation, respectively. Six karst fault and aquifer permeability ratio-working conditions are set up, and numerical simulation studies are conducted to reveal the Darcy-Brinkman-NS multifield coupled nonlinear seepage mechanism of karst fault synclines.

2. Nonlinear Mechanical Model of Three Flow Fields

The established nonlinear seepage model of three flow fields meets the following basic assumptions: the fault between the subsurface aquifer and the tunnel working surface is impermeable and serves as the only channel for fluid seepage; the porous media in aquifers and faults are isotropic; macroscopic fluid flow from the aquifer to the fault is a continuous process; the fluid in the model is incompressible, and the effect of temperature is neglected; and the fluid density and viscosity are constants.

2.1. Darcy Linear Flow in Aquifer. Fluids within deep rock-bearing aquifers are mainly driven by fluid pressure, and fluid inertia can be neglected [12]. Therefore, the fluid flow within this model's pressurized aquifer can be considered a low-velocity porous media seepage with a stable connection to the surrounding water source, which is described by Darcy's law in COMSOL Multiphysics.

$$\nabla \cdot (\rho u) = Q_m, \tag{1}$$

$$q = -\frac{k}{\mu}\nabla p, \tag{2}$$

where k is the permeability, p is the fluid pressure, ρ is the fluid density, Q_m is the source-sink term, q is the Darcy velocity, and μ is the dynamic viscosity.

2.2. Brinkman Equation in Fault Fracture Zone. The Brinkman equation is suitable for expressing the seepage characteristics in fault-fractured zone disturbed by excavation and is a nonlinear seepage equation between the Darcy flow and Navier-Stokes flow [13]. In COMSOL Multiphysics, the flow is described by the Brinkman equation with Forchheimer correction in the porous region.

$$q\left(\frac{\mu}{k} + \beta_f|q| + \frac{Q_{br}}{n}\right) = \nabla\left\{-pI + \frac{\mu}{n}\left[\nabla q + (\nabla q)^T\right]\right\} + F, \tag{3}$$

$$\rho\nabla \cdot (q) = Q_{br}, \tag{4}$$

where β_f is the non-Darcy factor, n is the porosity, F is the volume force affecting the fluid, and I is the unit matrix. According to the literature, the non-Darcy factor is obtained from the empirical formula [14].

$$\beta_f = \frac{0.005}{n^{5.5}\sqrt{k}}. \tag{5}$$

The relationship between the Forchheimer coefficient and the non-Darcy factor is

$$c_f = \beta_f\sqrt{k}. \tag{6}$$

2.3. Navier-Stokes Turbulent Flow in Roadway. The fault is under seepage migration, water-carrying particles gradually approaching the working face. When disturbed by mining or sufficient water volume, it is possible to break through the working face into the roadway free flow by the Navier-Stokes equation [15].

$$\rho(q \cdot \nabla)q = \nabla \cdot \left\{-pI + \mu\left[\nabla q + (\nabla q)^T\right]\right\} + F, \tag{7}$$

$$\rho\nabla \cdot q = 0. \tag{8}$$

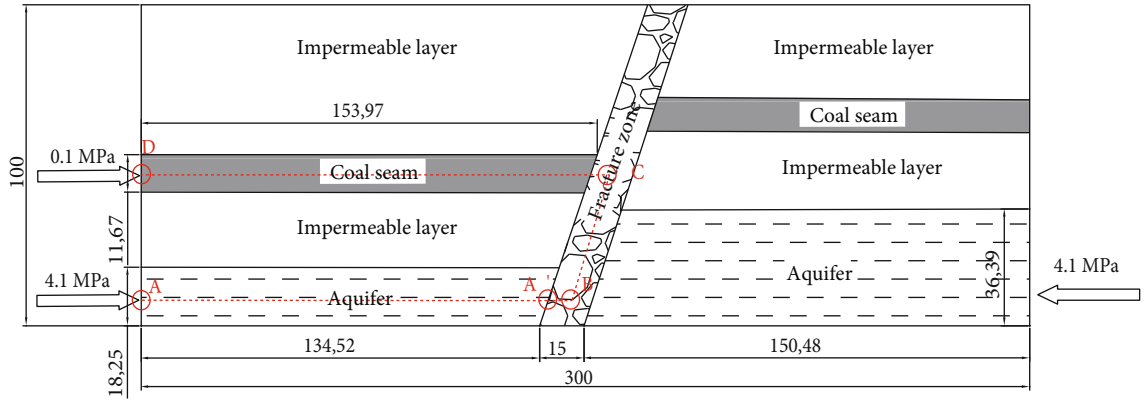

Figure 2: Numerical model of water inrush in Qiyue Mountain tunnel (unit: m).

Table 1: The hydrodynamic parameters in three stages.

Flow field parameters	Aquifer	Fault zone	Inside the tunnel
Density $p_w/kg \cdot m^{-3}$	1000	1000	1000
Power viscosity $\mu/Pa \cdot s$	0.001	0.001	0.001
Porosity of rock layer φ_s	0.14	0.348	—
Penetration rate k/m^2	2.1×10^{-11}	k_b	—
Non-Darcy factor β_f	—	Equation (5)	—
Initial pressure p_w/MPa	4.1	—	0.1

2.4. Boundary Conditions and Transition Conditions. The process of water entering the fault workings and gushing into the roadway from the pressurized aquifer in the process of water bursting from the fault can be simplified into three stages, as shown in Figure 1. These three stages are an organically linked unified whole, interacting and inseparable. Based on the mass conservation and pressure balance, the flow velocity and pressure of fluids in two adjacent regions are equal, the water pressure at the boundary of Darcy flow is constant, and the ambient atmospheric pressure is 0.1 MPa.

On the adjacent boundaries of aquifers and fault fracture zones, there are

$$p_{dl} = p_{br}, \tag{9}$$

$$u_{br} = u_{dl}. \tag{10}$$

On the adjacent boundary of the fault fracture zone and coal seam working face, there are

$$p_{br} = p_{ns}, \tag{11}$$

$$u_{ns} = u_{br}, \tag{12}$$

where the subscript D represents Darcy linear flow, B represents Brinkman nonlinear flow, and N represents Navier-Stokes turbulent flow.

Equations (1)–(12) jointly establish the Darcy-Brinkman-NS multifield coupled nonlinear seepage theoretical model of karst fault syncline and use COMSOL Multiphysics finite element software to develop the numerical model of three flow field coupled nonlinear seepage and analyze the characteristics of the seepage field at each stage by combining with actual engineering.

3. Numerical Modeling of Water Inrush in Fault Fracture Zone

This paper uses the F66 fault in the coal mine as an engineering background. F66 is one of the primary faults controlling the coal seam and structure of the coal mine, located on the north side of the thriving field, crossing the sound field from north to south, and is a positive fault in nature. The fault is cutting the coal seam, and the integrity of the coal seam has been damaged. The F66 spot has a significant drop, a wide fault width, and severe fragmentation.

According to the solid engineering background of the F66 fault in the coal mine, the numerical model of two-dimensional fault burst water is established by appropriate simplification. The model is 300 m long and 100 m wide, with three fluid stages corresponding to aquifer, fault, and roadway. The aquifer is located in the lower part of the model, divided into two trapezoids by the spot, with a fault break zone in the middle, 15 m wide and 70° inclination, and the coal seam is excavated from the left boundary, with an excavation working face height of 5 m. Detailed data are shown in Figure 2.

According to the hydrogeological conditions of the site, the seepage boundary of the model is set. The boundary on both sides of the aquifer is a fixed water pressure boundary with a water pressure of 4.1 MPa, the upper and lower boundaries are nonflowing boundaries, and the other outer boundaries of the model are nonflowing boundaries. There are $p_D = p_B$ and $u_D = u_B$ on the adjacent boundaries of the aquifer and fault fragmentation zone and $p_B = p_N$ and $u_B = u_N$ on the adjacent edges of the fault and the roadway. The upper part of the stress field is a fixed constraint boundary;

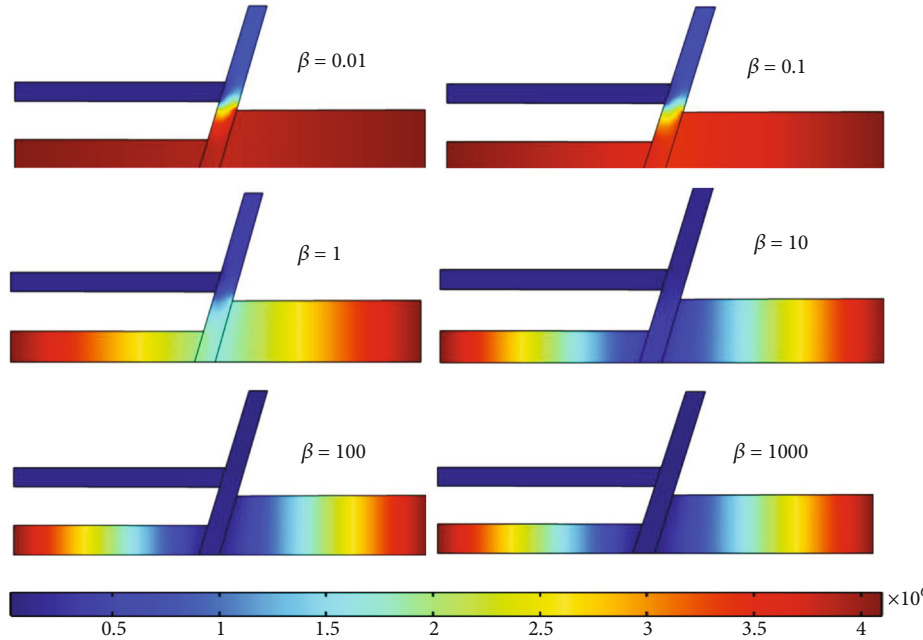

Figure 3: Fluid pressure profile under different gamma.

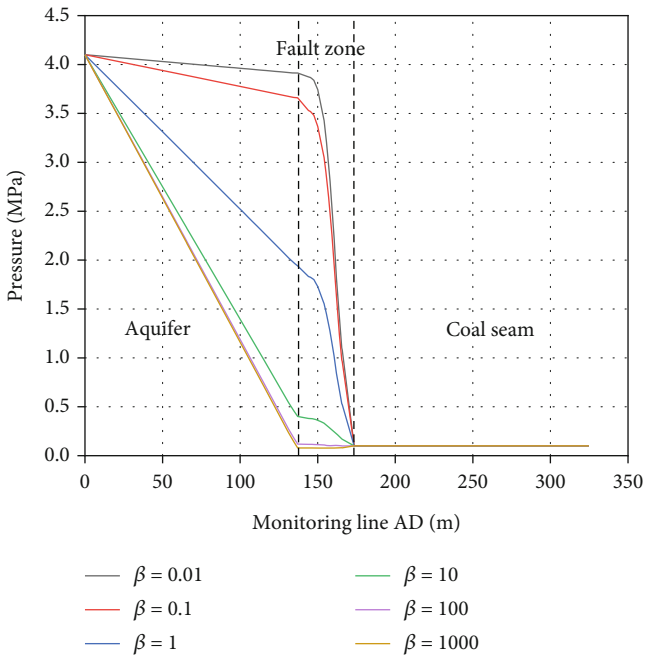

Figure 4: The pressure at each position on the A-D segment.

the two sides are rolling support boundaries, the excavation palm face and the prograde face are free boundaries, and the atmospheric pressure at the left edge of the coal seam tunnel is constant at 0.1 MPa.

Combining the established coupled nonlinear seepage model of three flow fields and the solid engineering background, the numerical model was based on using the finite element software COMSOL Multiphysics. The numerical model contains 358 domain cells and 203 edge cells, and the pressure and velocity of the three flow fields were calculated using the steady-state solver. Monitoring lines A-B-C-D record the changes in water pressure and flow velocity within the three flow fields. The aquifer permeability is 2.1×10^{-11} m^2, and the permeability of the fault fracture zone is a dynamic changing value, so β is set as the ratio of fault permeability to aquifer permeability. Six working conditions are placed in the numerical model; β values are 0.01, 0.1, 1, 10, 100, and 1000, respectively. The hydrodynamic parameters of the three stages are shown in Table 1.

4. Analysis of Simulation Results

4.1. Pressure and Flow Rate. Figure 3 shows a cloud of fluid pressure distribution for different β values. During the seepage process, the pressure and flow rate continuously change. As the ratio of fault to aquifer permeability increases, the color of the cloud map at the common boundary between the aquifer and the spot gradually becomes blue, which indicates that the pressure at the adjacent border will decrease progressively as the fault permeability increases and the fluid pressure is converted into fluid power, making it easier for the fluid to enter the fault through the common boundary according to the water pressure continuity and energy conservation. The underground aquifer is stable when β is 0.01, 0.1, or 1. When β is ten or more, the pressure at the junction of the fault and aquifer is reduced, indicating that when the fault permeability is greater than the aquifer, it will affect fluid stability in the aquifer. As β increases, the fluid pressure distribution in the aquifer is gradually uneven, showing a step change. The pressure within the fault gradually decreases from an inconsistent to a uniform state, indicating that the spot has become a channel connecting the aquifer and the roadway-working surface. There is no change in the color of the cloud map in the roadway, and

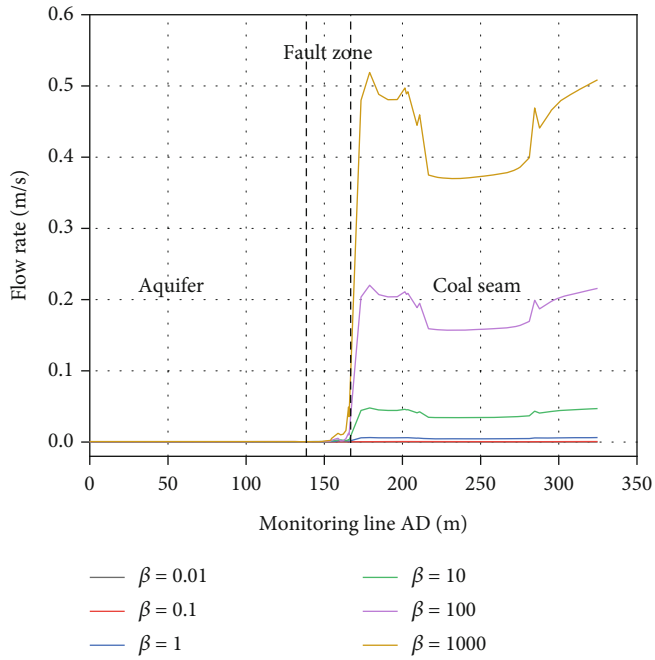

Figure 5: The velocity at each position on the A-D segment.

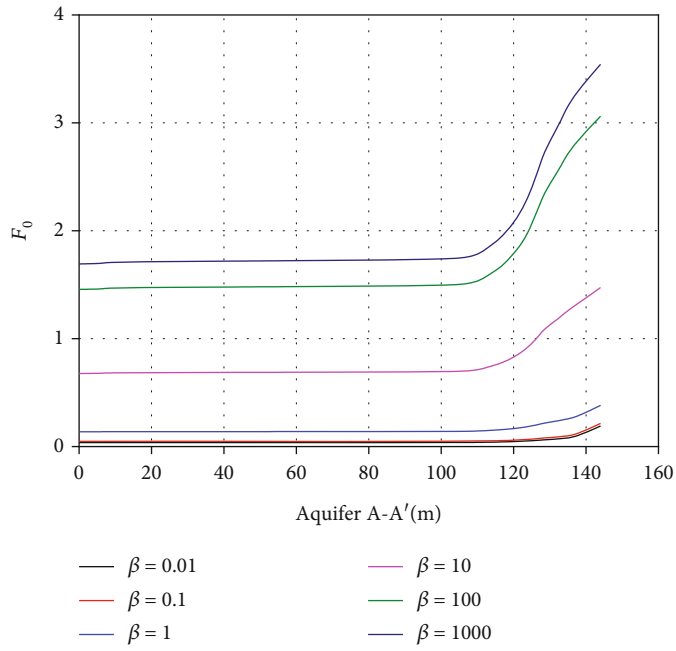

Figure 6: Forchhneimer number at different permeability ratios in aquifer A-A′.

the water pressure is always less than 0.1 MPa because the route is connected to the outside world and is kept as atmospheric pressure.

To understand more intuitively the changes of fluid pressure and velocity in aquifers, faults, and tunnels, the pressure and flow rate data on monitoring lines A-D obtained from numerical simulations were postprocessed to get the pressure versus velocity change curves. Figure 4 shows the variation curves of pressure at different β values for three stages on the monitoring line A-D. In the subsurface aquifer, the pressure decreases gradually and significantly with increasing β, and the pressure at the common boundary between the aquifer and the fault is also smaller. As the value increases, the rate of pressure drop in the fault gradually decreases, and when the β value is 1000, the pressure in the fault zone is stabilized at 0.1 MPa, which is

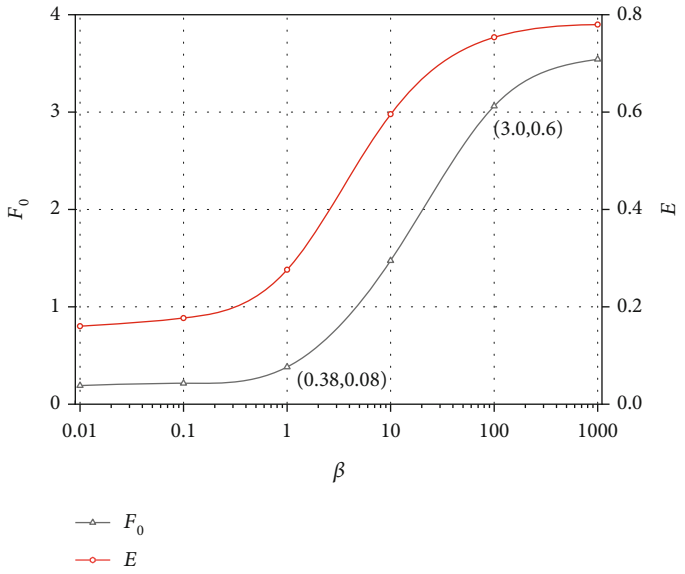

Figure 7: Forchhneimer number and non-Darcy effect E at point A′ at different permeabilities.

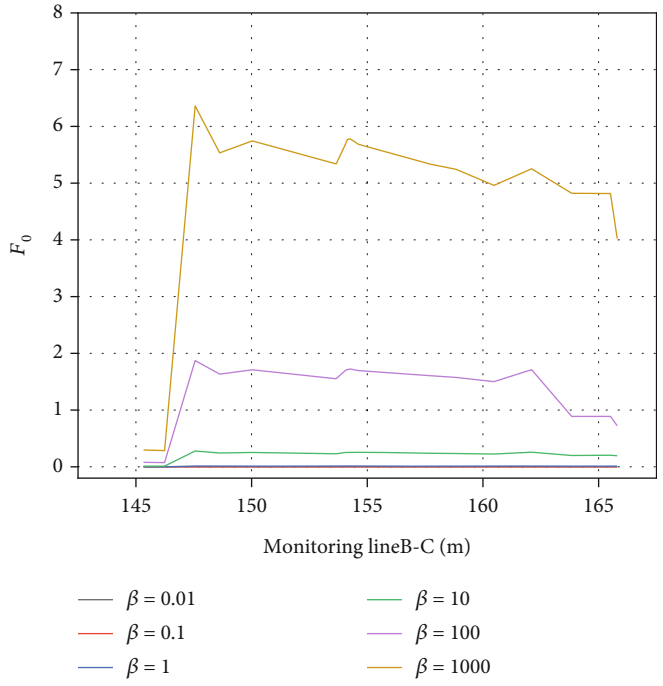

Figure 8: F_0 of fault zone BC under different permeability ratios.

basically unchanged. In the tunnel, the pressure does not vary with the value of β. The deal is close to the external atmospheric pressure of 0.1 MPa.

As can be seen from Figure 5, the fluid flow velocity in the underground aquifer and fault zone is small, and the flow velocity increases slightly at the common boundary. Fluid velocity in the fault and the roadway boundary shows a trend of rapid increase, and the flow velocity in the roadway fluctuates up and down, offering an unstable state, which indicates that the flow characteristics of the fluid in the roadway working surface change obviously and more suddenly, with the risk of sudden mud and water.

4.2. Non-Darcy Effect

4.2.1. Non-Darcy Flow Characteristics of the Aquifer. Darcy's law indicates that fluid pressure and flow velocity satisfy a linear relationship; however, the results in Figures 4 and 5 show that the aquifer pressure decreases with increasing β, while the flow velocity does not change significantly, and

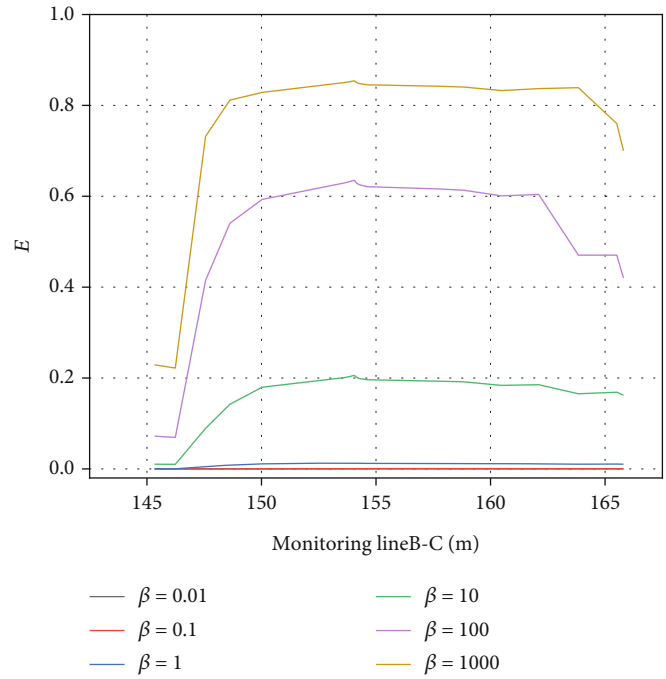

Figure 9: E of fault zone BC at different permeability ratios.

both pressure and flow velocity exhibit a nonlinear relationship; therefore, a quantitative value needs to be introduced to quantify the degree of fluid nonlinearity. Two methods are commonly used, namely, the ratio of gradients and the ratio of flow rates, which are mainly used [16, 17]. The Forchheimer number, which is the ratio of the quadratic term (fluid inertial term) to the primary term (fluid viscous term) in the Forchheimer equation [18, 19], reflects the degree of nonlinearity of fluid seepage and has been applied by scholars to discriminate the nonlinear seepage flow.

$$F_0 = \frac{\beta_f \rho |v_f| v_f}{(\mu/k) v_f} = \frac{\beta_f \rho k |v_f|}{\mu}. \tag{13}$$

The non-Darcy effects are

$$E = \frac{F_0}{1 + F_0}, \tag{14}$$

where β_f is the non-Darcy factor, calculated by *Eq.* k is the permeability; μ is the dynamic viscosity; v_f is the flow rate; and ρ is the density.

Figure 6 shows the Forchheimer number for different β values of the aquifer monitoring line A-A′ when β is 0.01, 0.1, and 1, $F_0 \ll 1$, indicating that when the fault permeability is small, the viscous resistance plays a dominant role in fluid flow, the liquid state is linear flow, and the fluid flow conforms to Darcy's law. And at $\beta = 10$, the value gradually increases as the fluid approaches the common boundary between the aquifer and the fault zone, indicating that inertia and viscosity jointly control the fluid flow at this time. The inertial resistance keeps increasing, and the viscous resistance gradually decreases from the leftmost side of the fluid to the common boundary position with the fault. The degree of fluid nonlinearity slowly increases. When β is 100 and 1000, the fault zone permeability is much larger than the aquifer permeability, more significant than 1, and the trend of growth is faster, rising to 3 at the common boundary, indicating that the increase of fault permeability gives a vital nonlinear characteristic to the flow of aquifer fluid.

Figure 7 shows F_0 and E at point A' on the aquifer monitoring line for different permeability ratios. As a whole, the two trends with increasing β values are close to the same. Specifically, both are increasing rapidly between $\beta = 1$ and $\beta = 100$, indicating a gradual increase in nonlinearity. After this, both slowly increase, eventually reaching a more stable value.

4.2.2. Non-Darcy Flow Characteristics of the Fault Zone. Figure 8 shows the fault zone BC at different permeability ratios, indicating that the Forchheimer number F_0 is small and tends to zero when $\beta \leq 10$, which suggests that the fluid flow is weakly nonlinear and tends to be linear in the fault zone. When $\gamma = 100$ or $\gamma = 1000$, F_0 increases significantly and is greater than the critical value of 1, indicating that the flow state of the fluid into the fault zone is nonlinear at larger permeabilities. Outside of the rapid increase and decrease in F_0 at both ends of the fault zone, this is due to the abrupt change in flow velocity at the common boundary. In addition, in the range of 147.5~165.5 on the monitoring line BC, the overall view of F_0 variation is small and relatively stable, indicating that the inertial resistance plays a dominant role in the fluid.

Figure 9 shows E in the fault zone BC at different permeability ratios because E varies with F_0. The analysis is similar to that of Figure 8. The fractured rock body of the fault contains many tiny rock and soil particles. The particles are continuously lost under fluid percolation migration, which

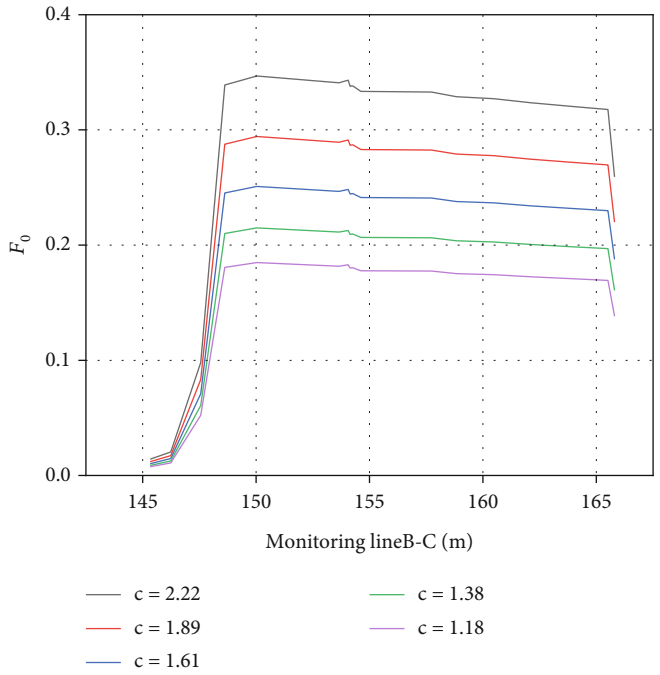

Figure 10: F_0 of the fault zone BC in the case of $\boldsymbol{\beta} = 10$ and different $\boldsymbol{c_f}$.

can cause changes in porosity and permeability. From Equations (6) and (7), the non-Darcy factor β_f and the Forchheimer coefficient c_f vary with the porosity. At a specific ratio of permeability γ, the fault zones have different porosity n, respectively, and the corresponding Forchheimer number of c_f is calculated. The effect of c_f on the fluid flow state can be analyzed. Therefore, $\beta = 10$ time, the average porosity of the fault zone is taken as 0.33, 0.34, 0.35, 0.36, and 0.37, respectively, to analyze the non-Darcy flow characteristics of the fault fracture zone.

Figure 10 shows the values of F_0 for BC in the fault zone at different Forchheimer coefficients at $\beta = 10$. For each c_f, the same phenomenon is that F_0 increases rapidly from an initial value approximately equal to zero when the fluid first enters the fault zone, is more stable when flowing in the fault, and decreases rapidly when rushing out of the guilt. In this process, the viscous resistance weakens, the inertial resistance increases, and the flow state of the fluid changes from linear to nonlinear flow. In the starting phase, the larger c_f is, the more significant the increase in F_0 is. The fluid with a larger c_f has a more considerable F_0 value at the exact location. At a specific ratio of permeability β, the larger the c_f of the fault affected by porosity, the larger the fluid tends to be in a nonlinear flow state.

5. Conclusions

(1) Through the study of pressure and flow velocity under six working conditions, as the permeability of the fault increases, the water pressure of the aquifer decreases, the speed of fluid entering the fault increases, and the water pressure of the aquifer changes from a stable state to a nonstable state, the affected area is expanded, and the water pressure of the fault changes from a nonstable state to a steady state. In the adjacent flow field area, the water pressure and flow velocity change abruptly, and the pore structure and the permeability of fault fracture zone are essential factors affecting the danger of water inrush

(2) As the permeability ratio increases, the fluid flow in the aquifer gradually changes from viscous resistance playing a dominant role to inertial resistance playing a dominant position. The Forchheimer number increases rapidly when the fluid flows through the adjacent area of the two flow fields. The Forchheimer number is more stable when it flows in the fault fracture zone, and the non-Darcy effect increases with the increase of the permeability ratio value. As the permeability of the fault increases, the fluid in the aquifer and the spot gradually changes from a linear flow state to a nonlinear flow state, and the nonlinear flow of fluid in the roadway shows prominent nonlinear characteristics

Data Availability

The data used to support the findings of this study are included within the article.

Conflicts of Interest

The authors declare that they have no conflicts of interest.

Acknowledgments

This work is supported by the National Natural Science Foundation of China (52274079 and U1904128), the Program for the Scientific and Technological Innovation Team in Universities of Henan Province (23IRTSTHN005), the Young Teacher Foundation of Henan Polytechnic University (2019XQG-08), and the Research and Practice Project of Educational and Teaching Reformation of Henan Polytechnic University (2021JG100).

References

[1] X. Z. Li, G. U. Luo, and Z. S. Chen, "Fracture deformation activation hydraulic conductivity mechanism of underground engineering sudden water," *Journal of Geotechnical Engineering*, vol. 24, no. 6, pp. 695–700, 2002.

[2] F. Li, J. N. Wang, and X. H. Wei, "Characteristics of rock fracture and hydraulic conductivity in the bottom slab of mining adjacent to a fault on a pressurized water body," *China Production Safety Science and Technology*, vol. 10, no. 5, pp. 68–73, 2014.

[3] C. H. Huang, G. C. Wen, J. J. Huang, and Y. S. Deng, "Characteristic analysis study of sudden water of Zhangcun mine fault," *Coal Engineering*, vol. 45, no. 6, pp. 90–92, 2013.

[4] E. T. Guan, "Characteristics of sudden water of fault in Yanmazhuang coal mine and its prediction method," *Coal Engineering*, vol. 61, no. 7, pp. 43–45, 2005.

[5] L. J. Li, M. J. Qian, and S. G. Li, "Analysis of the mechanism of fault sudden water," *Journal of Coal*, vol. 21, no. 2, p. 5, 1996.

[6] Z. J. Liu and Y. Q. Hu, "Study on solid-flow coupling of sudden water in coal mining faults on pressurized water," *Journal of Coal*, vol. 32, no. 10, pp. 1046–1050, 2007.

[7] L. C. Li, C. N. Tang, Z. Z. Liang, T. H. Ma, and Y. B. Zhang, "Simulation analysis of the formation process of burst water channel in the bottom plate of coal seam containing fault," *Journal of Rock Mechanics and Engineering*, vol. 28, no. 2, pp. 290–297, 2009.

[8] Q. F. Li, W. J. Wang, C. H. Zhu, and W. Q. Peng, "Analysis of the mechanism of fault sudden water based on the principle of water barrier key layer," *Journal of Mining and Safety Engineering*, vol. 26, no. 1, pp. 87–90, 2009.

[9] Z. Z. Cao, Y. F. Xue, H. Wang, J. R. Chen, and Y. L. Ren, "The non-Darcy characteristics of fault water inrush in karst tunnel based on flow state conversion theory," *Thermal Science*, vol. 25, no. 6, pp. 4415–4421, 2021.

[10] Z. Z. Cao, Y. Wang, H. X. Lin, Q. Sun, X. G. Wu, and X. S. Yang, "Hydraulic fracturing mechanism of rock mass under stress-damage-seepage coupling effect," *Geofluids*, vol. 2022, Article ID 5241708, 11 pages, 2022.

[11] Z. Z. Cao, Y. L. Ren, Q. T. Wang, B. H. Yao, and X. C. Zhang, "Evolution mechanism of water-conducting channel of collapse column in karst mining area of southwest China," *Geofluids*, vol. 2021, Article ID 6630462, 8 pages, 2021.

[12] T. H. Yang, S. G. Chen, W. C. Zhu, Z. P. Meng, and Y. F. Gao, "A preliminary investi gation on the mechanism of water breakout and nonlinear seepage model of mine rock destruction," *Journal of Rock Mechanics and Engineering*, vol. 26, no. 7, pp. 1411–1416, 2008.

[13] T. H. Yang, W. H. Shi, H. L. Liu, B. Yang, X. Yang, and Z. B. Liu, "Nonlinear seepage model based on flow transitions and its application in the analysis of water burst mechanism in trap columns," *Journal of Coal*, vol. 42, no. 2, pp. 315–321, 2017.

[14] J. Geertsma, "Estimating the coefficient of inertial resistance in fluid flow through porous media," *Society of Petroleum Engineers Journal*, vol. 14, no. 5, pp. 445–450, 1974.

[15] G. Q. Chen, T. B. Li, Z. F. Fan, and C. X. Yang, "Simulation of karst tunnel surge water process based on different seepage flow equations," *Hydrogeology and Engineering Geology*, vol. 38, no. 4, pp. 8–13, 2011.

[16] Y. F. Chen and J. Q. Zhou, "Evaluation of Forchheimer equation coefficients for non-Darcy flow in deformable rough-walled fractures," *Journal of Hydrology*, vol. 529, no. 3, pp. 993–1006, 2015.

[17] Q. Z. Jia and S. H. Hu, "The friction factor in the Forchheimer equation for rock fractures," *Rock Mechanics and Rock Engineering*, vol. 49, no. 8, pp. 3055–3068, 2016.

[18] Y. Xue, P. G. Ranjith, F. Gao, Z. Zhang, and S. Wang, "Experimental investigations on effects of gas pressure on mechanical behaviors and failure characteristic of coals," *Journal of Rock Mechanics and Geotechnical Engineering*, vol. 15, no. 2, pp. 412–428, 2023.

[19] Y. Xue, S. Liu, J. Chai et al., "Effect of water-cooling shock on fracture initiation and morphology of high-temperature granite: Application of hydraulic fracturing to enhanced geothermal systems," *Applied Energy*, vol. 337, p. 120858, 2023.